



HAL
open science

Spin-orbit splitting of Andreev states revealed by microwave spectroscopy

L Tosi, C Metzger, M F Goffman, C. Urbina, H. Pothier, Sunghun Park, A
Levy Yeyati, J. Nygård, P. Krogstrup

► **To cite this version:**

L Tosi, C Metzger, M F Goffman, C. Urbina, H. Pothier, et al.. Spin-orbit splitting of Andreev states revealed by microwave spectroscopy. 2018. hal-01888992v1

HAL Id: hal-01888992

<https://hal.science/hal-01888992v1>

Preprint submitted on 12 Oct 2018 (v1), last revised 13 Dec 2018 (v2)

HAL is a multi-disciplinary open access archive for the deposit and dissemination of scientific research documents, whether they are published or not. The documents may come from teaching and research institutions in France or abroad, or from public or private research centers.

L'archive ouverte pluridisciplinaire **HAL**, est destinée au dépôt et à la diffusion de documents scientifiques de niveau recherche, publiés ou non, émanant des établissements d'enseignement et de recherche français ou étrangers, des laboratoires publics ou privés.

Spin-orbit splitting of Andreev states revealed by microwave spectroscopy

L. Tosi, C. Metzger, M. F. Goffman, C. Urbina, and H. Pothier*
*Quantronics group, Service de Physique de l'État Condensé (CNRS, UMR 3680),
IRAMIS, CEA-Saclay, Université Paris-Saclay, 91191 Gif-sur-Yvette, France*

Sunghun Park and A. Levy Yeyati
*Departamento de Física Teórica de la Materia Condensada,
Condensed Matter Physics Center (IFIMAC) and Instituto Nicolás Cabrera, Universidad Autónoma de Madrid, Spain*

J. Nygård¹ and P. Krogstrup^{1,2}
¹ *Center for Quantum Devices,*
² *Microsoft Quantum Materials Lab,
Niels Bohr Institute, University of Copenhagen,
Copenhagen, Denmark*
(Dated: October 4, 2018)

We have performed microwave spectroscopy of Andreev states in superconducting weak links tailored in an InAs-Al (core-full shell) epitaxially-grown nanowire. The spectra present distinctive features, with bundles of four lines crossing when the superconducting phase difference across the weak link is 0 or π . We interpret these as arising from zero-field spin-split Andreev states. A simple analytical model, which takes into account the Rashba spin-orbit interaction in a nanowire containing several conduction channels, explains these features and their evolution with magnetic field. Our results show that the spin degree of freedom is addressable in Josephson junctions, and constitute a first step towards its manipulation.

Introduction. The Josephson supercurrent that flows through a weak link between two superconductors is a direct and generic manifestation of the coherence of the many-body superconducting state. The link can be a thin insulating barrier, a small piece of normal metal, a constriction or any other type of coherent conductor, but regardless of its specific nature the supercurrent is a periodic function of the phase difference δ between the electrodes [1]. However, the exact function is determined by the geometry and material properties of the weak link. A unifying microscopic description of the effect has been achieved in terms of the spectrum of discrete quasiparticle states that form at the weak link: the Andreev bound states (ABS) [2–4]. The electrodynamics of an arbitrary Josephson weak link in a circuit is not only governed by the phase difference but depends also on the occupation of these states. Spectroscopy experiments on carbon nanotubes [5], atomic contacts [6–8] and semi-conducting nanowires [9–11] have clearly revealed these fermionic states, each of which can be occupied at most by two quasiparticles. The role of spin in these excitations is a topical issue in the rapidly growing fields of hybrid superconducting devices [12, 13] and of topological superconductivity [14–17]. It has been predicted that for finite length weak links the combination of a phase difference, which breaks time-reversal symmetry, and of spin-orbit coupling, which breaks spin-rotation symmetry, is enough to lift the spin degeneracy, giving therefore rise to spin-dependent Josephson supercurrents [18–21]. Here we report the first observation of transitions between zero-field spin-split ABS.

ABSs and spin-orbit interaction. Andreev bound

states are formed from the coherent Andreev reflections that quasiparticles undergo at both ends of a weak link. Quasiparticles acquire a phase at each of these Andreev reflections and while propagating along the weak link of length L . Therefore, the ABS energies depends on δ , on the transmission probabilities for electrons through the weak link and on the ratio $\lambda = L/\xi$ where ξ is the superconducting coherence length. Assuming ballistic propagation, $\xi = \hbar v_F/\Delta$ is given in terms of the velocity v_F of quasiparticles at the Fermi level within the weak link and of the energy gap Δ of the superconducting electrodes. In a short junction, defined by $L \ll \xi$, each conduction channel of the weak link, with transmission probability τ , gives rise to a single spin-degenerate Andreev level at energy $E_A = \Delta\sqrt{1 - \tau \sin^2(\delta/2)}$ [2–4]. This simple limit has been probed in experiments on aluminum superconducting atomic contacts, using three different methods: Josephson spectroscopy [6], switching current spectroscopy [7] and microwave spectroscopy in a circuit-QED setup [8]. The spectrum of Andreev states in a weak link with a sizable spin-orbit coupling has already been probed in two experiments on InAs nanowires [10, 11]. Both experiments were performed in the limit $L \lesssim \xi$. In Ref. [11], the zero field spectrum was probed using a circuit-QED setup and no effect of spin-orbit interaction was reported. In Ref. [10], where spectra at finite field were obtained by Josephson spectroscopy, spin-orbit interaction enters in the interpretation of the spectra when the Zeeman energy is comparable to the superconducting gap [22].

In a one-dimensional weak link, spin-orbit interaction

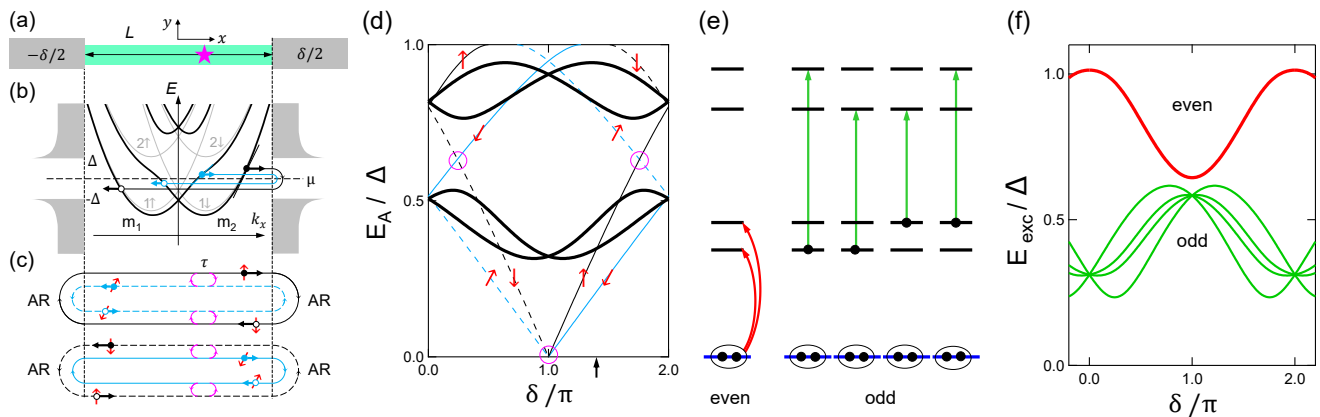


FIG. 1. Effect of the Rashba spin-orbit coupling on Andreev levels. (a) Nanowire of length L forming a weak link between superconductors with phase difference δ . Magenta star symbolizes a scatterer. (b) Dispersion relation for a nanowire considering just two transverse subbands in the presence of Rashba spin-orbit (RSO) coupling. A first effect of RSO is to spin-split the parabolic dispersion relations along the k_x axis (grey solid lines labelled $1\uparrow\downarrow$ and $2\uparrow\downarrow$ with \uparrow and \downarrow indicating the spin in the y -direction). In addition, RSO couples states of different subbands and opposite spins leading to avoided crossings. The resulting bands (black solid lines) have an energy-dependent spin texture. The Fermi level μ is such that only the lowest energy bands m_1 and m_2 are occupied. The density of states of the superconducting electrodes is sketched at both ends of the wire. Andreev reflection (AR) on the superconductors couples electrons (full circles) with holes (open circles) with opposite spin and opposite velocities, *i.e.* time-reversed partners. This is illustrated for right-moving electrons which have different velocities: a fast electron (in black) from m_2 and a slow electron (light blue) from m_1 . (c) Andreev reflections at both ends lead to the formation of Andreev bound states (ABS), which in the absence of normal scattering form two distinct families. The spin of these electrons, schematized with red arrows, is pointing in a different direction as a consequence of the spin texture of the bands. (d) Energy of ABS. Thin black and light blue lines correspond to ballistic case. In (c) and (d), thin solid lines correspond to right-moving electrons and left-moving holes, and dashed lines the opposite. Backscattering in the nanowire (indicated with magenta arrows in (c)) couples right- and left-moving electrons (holes) within each band m_1 or m_2 , leading to the lifting of degeneracy at the crossings highlighted with magenta circles in (d). The resulting Andreev levels (black solid lines) group in two manifolds. (e) Energy spectrum at a particular phase difference indicated with a black arrow in the bottom axis of (d), and possible microwave-induced transitions. The pair of red arrows correspond to an *even* transition in which the system is initially in the ground state and two quasiparticles are created in the first ABS manifold. The green arrows correspond to *odd* transitions where a trapped quasiparticle is promoted from the first to the second ABS manifold. (f) Expected excitation spectrum as a function of the phase.

does not break the spin degeneracy of ABSs since the spatial phase acquired by the electron and the Andreev-reflected hole is the same for both spin directions [23, 24]. This is no longer the case in presence of a second transverse subband, even if just the lowest one is actually occupied [24–28]. In Fig. 1 we consider a weak link described by two subbands and show the effect of a strong spin-orbit coupling. Rashba spin-orbit interaction lifts the spin degeneracy and couples the subbands, leading to four spinful bands (Fig. 1(b)). We focus on a situation in which the Fermi level is such that only the two lowest ones (m_1 and m_2 in the figure) are occupied. Quasiparticles at the Fermi level have different velocities and different spin textures in each band. Imposing that the phase accumulated along the closed paths depicted in Fig. 1(c) is a multiple of 2π , one obtains the ABSs represented by the thin lines in Fig. 1(d). In presence of backscattering in the nanowire, due either to impurities or to the spatial variation of the electrostatic potential along the wire, electrons (as well as holes) travelling in opposite directions are coupled, opening gaps at the points indicated by the open circles in Fig. 1(d). The resulting ABSs

group in manifolds of spin-split states represented by the thick black lines. In the absence of a magnetic field, the states remain degenerate at $\delta = 0$ and π , as expected by time-reversal symmetry. Figure 1(e) shows parity-conserving transitions that can be induced by absorption of a microwave photon, at a given phase. The red arrows correspond to an *even* transition in which the system is initially in the ground state and two quasiparticles are created in the first ABS manifold. The green arrows correspond to *odd* transitions where a trapped quasiparticle [29] occupying the first ABS manifold is excited to the second one [24, 30]. The corresponding transition energies in the absorption spectrum for both the *even* and *odd* cases are shown in Fig. 1(f), as a function of the phase difference. The even transition does not carry information on the spin structure. On the contrary, the peculiar feature formed by the possible odd transitions, as a bundle of four distinct lines all crossing at $\delta = 0$ and $\delta = \pi$, is a direct signature of the spin splitting of the states.

Figure 2 shows a spectrum measured on an InAs weak link with aluminum electrodes. The plot shows at which

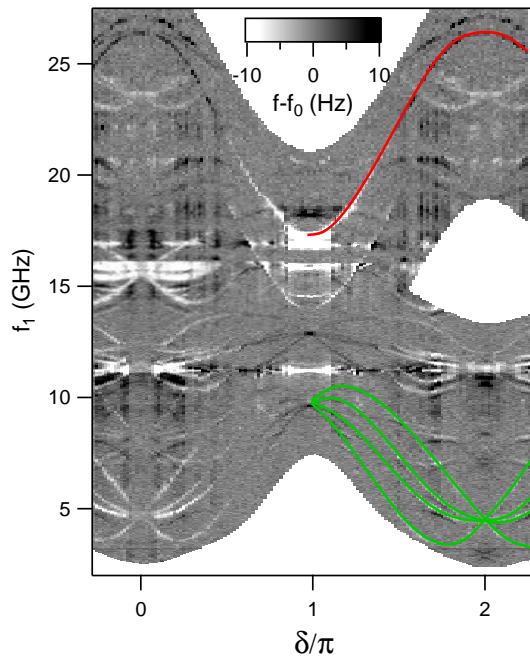


FIG. 2. Microwave excitation spectrum measured at a gate voltage $V_g = -0.89$ V. The grey scale represents the frequency change $f - f_0$ of a resonator coupled to the weak link when a microwave excitation at frequency f_1 is applied, as a function of the phase difference δ across the weak link. In the right half of the figure, some transition lines are highlighted. Red line corresponds to an *even* transition, green lines are *odd* transitions.

frequency f_1 microwave photons are absorbed, as a function of the phase difference δ across the weak link (see description of the experiment below). This is a very rich spectrum, but here we point two salient features highlighted with color lines on the right half side of the figure. The red line corresponds to an *even* Andreev transition, with extrema at $\delta = 0$ and $\delta = \pi$. The frequency $f_1(\delta = 0) = 26.5$ GHz is much smaller than twice the gap of aluminum $2\Delta/h = 88$ GHz, as expected for a junction longer than the coherence length. To the best of our knowledge, this is the first observation of a discrete Andreev spectrum in the long-junction limit. The observation of the bundle of lines (in green) with crossings at $\delta = 0$ and $\delta = \pi$ that clearly correspond to the *odd* transitions shown in Fig. 1(f) is the central result of this work.

Experimental setup. The measurements are obtained using the circuit-QED setup shown in Fig. 3(d), and performed at ~ 40 mK in a pulse-tube dilution refrigerator. The superconducting weak link was obtained by etching away, over a 370-nm-long section, the 25-nm-thick aluminum shell that fully covers a 140-nm-diameter InAs nanowire [31, 32] (see Figs. 3(a) and (b)). A side-gate allows tuning the charge carrier density and the electrostatic potential in the nanowire and therefore the An-

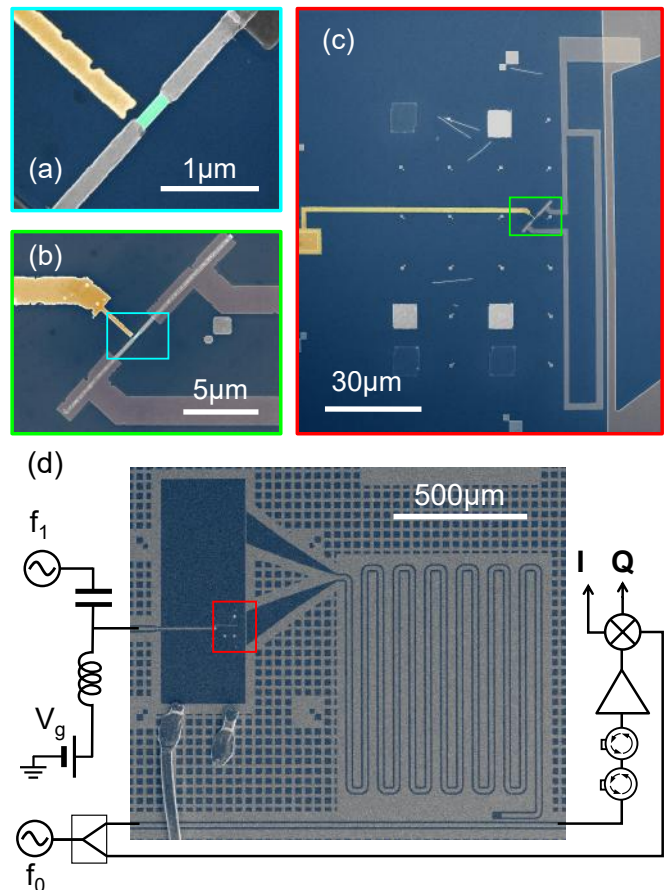


FIG. 3. Experimental setup. (a) False-color scanning electron microscope image of the InAs-Al core-shell nanowire. The Al shell (grey) was removed over 370 nm to form the weak link between the superconducting electrodes. A close-by side electrode (Au, yellow) is used to gate the InAs exposed region (green). (b),(c) The nanowire is connected to Al leads that form a loop. This loop is located close to the shorted end of a coplanar wave guide (CPW) resonator. (d) The CPW resonator is probed by sending through a bus line a continuous microwave tone at its resonant frequency $f_0 = 3.26$ GHz and demodulating the transmitted signal, yielding quadratures I and Q . Microwaves inducing Andreev transitions are applied through the side gate (frequency f_1) using a bias tee, the DC port being used to apply a DC voltage V_g .

dreev spectra [10]. The weak link is part of an aluminum loop of area $S \sim 10^3 \mu\text{m}^2$, which has a connection to ground to define a reference for the gate voltage (see Fig. 3(c)). The phase δ across the weak link is imposed by a magnetic field B_z perpendicular to the sample plane: $\delta = B_z S / \varphi_0$, with $\varphi_0 = h/2e$ the reduced flux quantum. Two additional coils are used to apply a magnetic field in the plane of the sample. The loop is inductively coupled to the shorted end of a $\lambda/4$ microwave resonator made out of Nb, with resonance frequency $f_0 \approx 3.26$ GHz and internal quality factor $Q_{\text{int}} \approx 10^6$. A continuous signal at frequency f_0 is sent through a coplanar transmission line coupled to the resonator (coupling quality factor

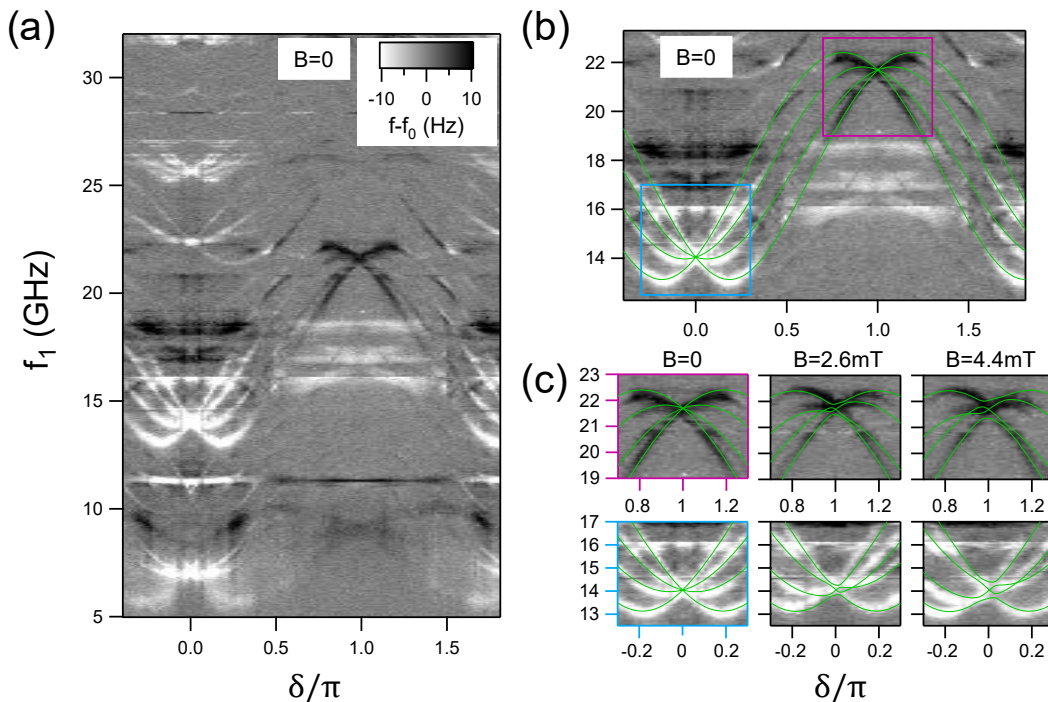


FIG. 4. Excitation spectra at $V_g = 0.5$ V. (a) Large scale spectrum at zero magnetic field. (b) Zoom on the same data, with fits (see text). (c) Dependence of the spectrum with the amplitude B of an in-plane magnetic field applied at an angle of -45° with respect to the nanowire axis. Green lines are fits (see text).

$Q_c \approx 1.7 \times 10^5$), and the two quadratures I and Q of the transmitted signal are measured using homodyne detection (see Fig. 3(d)). Andreev excitations in the weak link are induced by a microwave signal of frequency f_1 applied on the side gate. The corresponding microwave source is chopped at 3.3 kHz, and the response in I and Q is detected using two lock-ins, with an integration time of 0.1 s. The fact that *odd* transitions are observed (see Fig. 2) means that during part of the measurement time Andreev states are occupied by a single quasiparticle. This is in agreement with previous experiments, in which the fluctuation rates for the occupation of Andreev states by out-of-equilibrium quasiparticles were found to be in the 10 ms^{-1} range [8, 11, 29]. Note that in contrast to an excitation that couples to the phase across the contact [8, 22, 24], exciting through the gate allows transitions away from $\delta = \pi$ and at frequencies very far detuned from that of the resonator.

Spectroscopy at zero magnetic field. Figure 4(a) presents another spectrum taken at zero magnetic field (apart from the tiny perpendicular field $B_z < 5 \mu\text{T}$ required for the phase biasing of the weak link), at $V_g = 0.5$ V. In comparison with the spectrum in Fig. 2, *even* transitions are hardly visible in Fig. 4. Bundles of lines corresponding to *odd* transitions have crossings at 7.1, 14.0 and 22.4 GHz at $\delta = 0$ and 9, 21.5 and 26.0 GHz at $\delta = \pi$. Here, as in Fig. 2, replica of transition lines shifted by f_0 are also visible. They correspond to transi-

tions involving the absorption of a photon from the resonator. We focus on the bundle of lines between 13 and 23 GHz for which the effect of a magnetic field B was also explored. Green lines in Fig. 4(b) are fits of the data at $B = 0$ with a simple model that accounts for two bands with different Fermi velocities v_1 and v_2 , and the presence of a single scatterer in the wire (see Appendix). The model parameters are $\lambda_{j=1,2} = L\Delta/(\hbar v_j)$ and the position $x_0 \in [-L/2, L/2]$ of the scatterer of transmission τ . ABSs are found at energies $E = \epsilon\Delta$, with ϵ solution of the transcendental equation:

$$\tau \cos((\lambda_1 - \lambda_2)\epsilon \mp \delta) + (1 - \tau) \cos((\lambda_1 + \lambda_2)\epsilon x_r) = \cos(2 \arccos \epsilon - (\lambda_1 + \lambda_2)\epsilon) \quad (1)$$

where $x_r = 2x_0/L$. The fit in Fig. 4(b) corresponds to $\lambda_1 = 1.3$, $\lambda_2 = 2.3$, $\tau = 0.295$ and $x_r = 0.525$ (we take $\Delta = 182 \mu\text{eV} = \hbar \times 44 \text{ GHz}$ for the gap of Al). These values can be related to microscopic parameters, in particular to the intensity α of the Rashba spin-orbit interaction entering in the Hamiltonian of the system as $H_R = -\alpha(k_x\sigma_y - k_y\sigma_x)$ (with $\sigma_{x,y}$ Pauli matrices acting in the spin) [24]. Assuming a parabolic transverse confinement potential, an effective wire diameter of $W = 140 \text{ nm}$, and an effective junction length of $L = 370 \text{ nm}$, the values of $\lambda_{1,2}$ are obtained for $\mu = 422 \mu\text{eV}$ (measured from the bottom of the band) and $\alpha = 38 \text{ meV nm}$, a value consistent with previous estimations [34, 35]. However, we stress that this estimation is model-dependent: very

similar fits of the data can be obtained using a double-barrier model (with scattering barriers located at the left ($x = -L/2$) and right ($x = L/2$) edges of the wire) with $\lambda_1 = 1.1$ and $\lambda_2 = 1.9$, leading to $\alpha = 32$ meV nm. For both models, we get only two manifolds of Andreev levels in the spectrum, and only these four odd transitions are expected in this frequency window (transitions within a manifold are all below 3.5 GHz). The other bundles of transitions are attributed to other conduction channels: although we considered till now only one occupied transverse subband, the same effect of spin-dependent velocities is found if several subbands cross the Fermi level. A more elaborate model, together with a realistic modelling of the bands of the nanowire, is required to treat this situation and obtain a quantitative fit of the whole spectra.

Spin character of ABS. While the splitting of the ABSs and the associated transitions in the absence of a Zeeman field reveals the difference in the Fermi velocities v_1 and v_2 , arising from the spin-orbit coupling in the multi-channel wire, it does not shine a light on the ABSs spin structure. This information can be inferred from the behavior of the bound states under a finite magnetic field, and in particular as a function of the orientation of the field with respect to the nanowire axis [24]. Figure 4(c) shows the spectrum in presence of an in-plane magnetic field with amplitudes $B = 0, 2.6$ and 4.4 mT applied at an angle of -45° with respect to the wire axis. The symmetry around $\delta = 0$ and $\delta = \pi$ is lost. This is accounted for by an extension of the single-barrier model at finite magnetic field (green lines) assuming a g-factor $g = 12$ (see Appendix).

The specific effects of a parallel and of a perpendicular magnetic field on the ABS are shown in Fig. 5. When the field is perpendicular to the wire ($B \perp x$), the ABS spectrum becomes asymmetric (this is related to the physics of φ_0 junctions [26]), as observed in Fig. 5(b,d). The field is directly acting in the quantization direction of the spin-split transverse subbands (gray parabolas in Fig. 1(b)) from which the ABS are constructed, leading to Zeeman shifts of the energies. Green lines are the result from the theory using the same parameters as in Fig. 4. When the field is along the wire axis $B \parallel x$, and thus perpendicular to the spin quantization direction, it mixes the spin textures and lifts partly the degeneracies at $\delta = 0$ and $\delta = \pi$ (see Fig. 6 in Appendix). The spectrum of ABS is then modified, but remains symmetric [36], around $\delta = 0$ and π , see Fig. 5(a,c).

Concluding remarks. The results reported here show that the quasiparticle spin can be a relevant degree of freedom in Josephson weak links, even in the absence of a magnetic field. This work leaves several open questions. Would a more realistic model allow for a precise characterization of spin-orbit interaction in the nanowire from the measured spectra? How to understand the coupling between the microwave photons and the ABS when

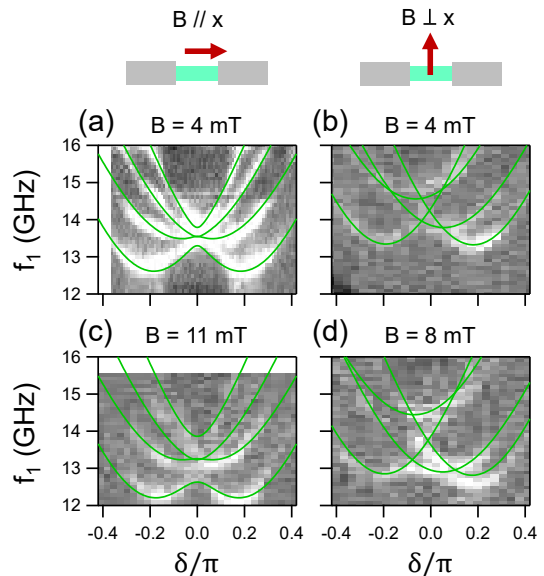


FIG. 5. Effect of an in-plane magnetic field on the ABS excitation spectrum around $\delta = 0$. The Andreev states correspond to the same gate voltage as in Fig. 4. Field is applied parallel (a,c) or perpendicular (b,d) to the wire. Green lines are the result from the theory (see text).

the excitation is induced through electric field, as done here, instead of phase modulation [24, 30, 38]? In particular, what are the selection rules? Are transitions between ABS belonging to the same manifold allowed? Can one observe *even* transitions leading to states with quasiparticles in different manifolds? What determines the signal amplitude? Independently of the answer to these questions, the observation of spin-resolved transitions between ABSs is a first step towards the manipulation of the spin of a single superconducting quasiparticle [18, 24]. It raises the question whether the spin coherence time of a localized quasiparticle is different from that of a propagating one [41]. Finally, we think that the experimental strategy used here could allow probing a topological phase with Majorana bound states at larger magnetic fields [30].

Technical support from P. Sénat is gratefully acknowledged. We thank A. Reynoso, Ç. Girit, H. Bouchiat, M. Devoret, M. Hays, K. Serniak, and our colleagues from the Quantronics group for useful discussions. We thank P. Orfila and S. Delprat for nanofabrication support. This work has been supported ANR contract JETS, by the Renatech network, by the Spanish MINECO through Grant No. FIS2014-55486-P, FIS2017-84860-R and through the “María de Maeztu” Programme for Units of Excellence in R&D (MDM-2014-0377). Center for Quantum Devices is supported by the Danish National Research Foundation. L.Tosi was supported by the Marie Skłodowska-Curie individual fellowship grant 705467. P. Krogstrup acknowledges support from Microsoft Quantum and the European Research Council

(ERC) under the grant agreement No.716655 (HEMs-DAM)

Appendix: Details on the theoretical model and the fitting parameters

The nanowire is described by 4 transverse subbands denoted by $n\sigma$, with $n = 1, 2$ and $\sigma = \uparrow, \downarrow$, arising from a confining harmonic potential in the transverse direction (gray parabolas in Fig. 1(b)) under the effect of Rashba spin-orbit coupling with intensity α . The energy dispersion relations of the resulting lowest subbands (black lines labelled m_1 and m_2 in Fig. 1(b)) are

$$E_s(k_x) = \frac{\hbar^2 k_x^2}{2m^*} + \frac{E_1^\perp + E_2^\perp}{2} - \sqrt{\left(\frac{E_1^\perp - E_2^\perp}{2} - s\alpha k_x\right)^2 + \eta^2}, \quad (2)$$

where $s = -1$ corresponds to m_1 and $s = +1$ to m_2 , and $E_n^\perp = 4\hbar^2 n / (m^* W^2)$ where W is the effective diameter of the nanowire and m^* is the effective mass. $\eta = \sqrt{2}\alpha/W$ is the strength of the subband mixing due to the Rashba spin-orbit coupling. Particle backscattering within the nanowire is accounted for by either a single delta-like potential barrier located at some arbitrary position x_0 or by potential barriers localized at both ends ($x = \pm L/2$).

The linearized Bogoliubov-de Gennes equation around the chemical potential μ is

$$\begin{pmatrix} H_0 + H_b & \Delta(x)e^{i\delta(x)} \\ \Delta(x)e^{-i\delta(x)} & -H_0 - H_b \end{pmatrix} \Psi(x) = E_A \Psi(x) \quad (3)$$

with the basis $\Psi(x) = (\psi_{+,R}^e(x), \psi_{+,L}^e(x), \psi_{-,R}^e(x), \psi_{-,L}^e(x), \psi_{+,R}^h(x), \psi_{+,L}^h(x), \psi_{-,R}^h(x), \psi_{-,L}^h(x))$, where $R(L)$ refers to the right-moving (left-moving) electron (e) or hole (h) in the bands $m_1(-)$, $m_2(+)$. Here H_0 is the Hamiltonian for electrons in the nanowire

$$H_0 = \begin{pmatrix} -i\hbar v_1 \partial_x - \hbar v_1 k_{F1} & 0 & 0 & 0 \\ 0 & i\hbar v_2 \partial_x - \hbar v_2 k_{F2} & 0 & 0 \\ 0 & 0 & -i\hbar v_2 \partial_x - \hbar v_2 k_{F2} & 0 \\ 0 & 0 & 0 & i\hbar v_1 \partial_x - \hbar v_1 k_{F1} \end{pmatrix}, \quad (4)$$

where $v_{j=1,2}$ are the Fermi velocities given by

$$v_j = \frac{\hbar k_{Fj}}{m^*} + (-1)^j \frac{\alpha (E_1^\perp/2 - (-1)^j \alpha k_{Fj})}{\sqrt{(E_1^\perp/2 - (-1)^j \alpha k_{Fj})^2 + \eta^2}}, \quad (5)$$

and k_{Fj} are the Fermi wave vectors satisfying $E_s(k_{Fj}) = \mu$. The potential scattering term H_b is modeled as

$$H_b = U_b(x) \begin{pmatrix} 1 & \cos[(\theta_1 - \theta_2)/2] & 0 & 0 \\ \cos[(\theta_1 - \theta_2)/2] & 1 & 0 & 0 \\ 0 & 0 & 1 & \cos[(\theta_1 - \theta_2)/2] \\ 0 & 0 & \cos[(\theta_1 - \theta_2)/2] & 1 \end{pmatrix}, \quad (6)$$

where

$$U_b(x) = \begin{cases} U_0 \delta(x - x_0) & \text{for a single barrier at } x = x_0 \\ U_L \delta(x + L/2) + U_R \delta(x - L/2) & \text{for barriers at } x = -L/2 \text{ and } x = L/2, \end{cases} \quad (7)$$

and $\theta_{j=1,2} = \arccos[(-1)^j (\hbar k_{Fj} / m^* - v_j) / \alpha]$ characterize the spin orientations of the modified subbands. The superconducting order parameter $\Delta(x)e^{i\delta(x)}$ in Eq. (3) is given by $\Delta e^{-i\delta/2}$ at $x < -L/2$, $\Delta e^{i\delta/2}$ at $x > L/2$, and zero otherwise, where δ is the superconducting phase difference.

Ballistic regime. In the absence of particle backscattering, the phase accumulated in the Andreev reflection processes at $x = -L/2$ and $x = L/2$, as illustrated in Fig. 1(c), leads to the following transcendental equation for the energy $\epsilon = E_A/\Delta$ of the ABSs as a function of δ :

$$\sin(\epsilon \lambda_1 - s\delta/2 - \arccos \epsilon) \sin(\epsilon \lambda_2 + s\delta/2 - \arccos \epsilon) = 0, \quad (8)$$

where $\lambda_{j=1,2} = L\Delta/(\hbar v_j)$. For $\epsilon \ll 1$, there are two sets of solutions given by

$$\begin{cases} \epsilon_{\uparrow}(\delta) = \frac{1}{1+\lambda_1} \left[\frac{\delta}{2} + \left(l + \frac{1}{2}\right) \pi \right] \\ \epsilon_{\downarrow}(\delta) = \frac{1}{1+\lambda_1} \left[-\frac{\delta}{2} + \left(l' + \frac{1}{2}\right) \pi \right] \end{cases},$$

$$\begin{cases} \epsilon_{\swarrow}(\delta) = \frac{1}{1+\lambda_2} \left[\frac{\delta}{2} + \left(l + \frac{1}{2}\right) \pi \right] \\ \epsilon_{\searrow}(\delta) = \frac{1}{1+\lambda_2} \left[-\frac{\delta}{2} + \left(l' + \frac{1}{2}\right) \pi \right] \end{cases},$$

with integers l and l' . The ballistic ABSs are represented by the thin lines (black and light-blue) in Fig. 1(d).

Single barrier model. In this case, the effect of the barrier can be taken into account as an additional boundary condition at $x = x_0$,

$$\Psi(x_0 + 0^+) = \begin{pmatrix} M_{12} & 0 & 0 & 0 \\ 0 & M_{21} & 0 & 0 \\ 0 & 0 & M_{12} & 0 \\ 0 & 0 & 0 & M_{21} \end{pmatrix} \Psi(x_0 - 0^+), \quad (9)$$

where 0^+ is a positive infinitesimal and M_{ij} is the 2×2 matrix given by

$$M_{ij} = \frac{1}{t'} \begin{pmatrix} tt' - rr' & \sqrt{\frac{v_j}{v_i}} r' e^{i\varphi} \\ -\sqrt{\frac{v_i}{v_j}} r e^{-i\varphi} & 1 \end{pmatrix} \quad (10)$$

with $\varphi = ((k_{F1} + k_{F2}) + (\lambda_1 + \lambda_2)\epsilon/L)x_0$. The reflection and transmission coefficients are determined by

$$\begin{aligned} t e^{-iu_a} &= t' e^{iu_a} = \left(\cos d + i u_s \frac{\sin d}{d} \right)^{-1}, \\ r e^{-i\varphi} &= r' e^{i\varphi} = -i \sqrt{u_1 u_2} \frac{\sin d}{d} \cos \left(\frac{\theta_1 - \theta_2}{2} \right) \sqrt{tt'}, \\ d &= \frac{1}{2} \sqrt{u_1^2 + u_2^2 - 2u_1 u_2 \cos(\theta_1 - \theta_2)}, \end{aligned} \quad (11)$$

where $v_0 = \hbar v_1 v_2 / U_0$, $u_j = v_j / v_0$, $u_s = (u_1 + u_2) / 2$, and $u_a = (u_1 - u_2) / 2$. From the continuity conditions at $x = \pm L/2$ and Eq. (9) we find the transcendental equation (1) where $\tau = |t|^2$.

Double barrier model. In this case, there are two boundary conditions similar as Eq. (9) at the NS interfaces, which results in the transcendental equation

$$\begin{aligned} \sin(\tilde{\epsilon}_1 - \arccos \epsilon) \sin(\tilde{\epsilon}_2 - \arccos \epsilon) &= (2 - \tau_L - \tau_R) \sin(\tilde{\epsilon}_1) \sin(\tilde{\epsilon}_2) \\ &\quad - (1 - \tau_L)(1 - \tau_R) \sin(\tilde{\epsilon}_1 + \arccos \epsilon) \sin(\tilde{\epsilon}_2 + \arccos \epsilon) \\ &\quad - 2\sqrt{(1 - \tau_L)(1 - \tau_R)} \cos(\varphi_{\text{tot}})(1 - \epsilon^2), \end{aligned} \quad (12)$$

where $\tilde{\epsilon}_j = \epsilon \lambda_j + (-1)^j s \delta / 2$, $\tau_{L,R}$ are the transmission probabilities at $x = \mp L/2$, θ_ν are the scattering phases acquired at the interfaces ($\nu \equiv L, R$):

$$\theta_\nu = \arg \left(\cos d_\nu + i \frac{\sin d_\nu}{d_\nu} \frac{v_s}{v_\nu} \right), \quad (13)$$

where d_ν and v_ν are defined as d in Eq. (11) replacing U_0 by U_ν . Finally, we note $\varphi_{\text{tot}} = (k_{F1} + k_{F2})L - (\theta_L + \theta_R)$ the total accumulated phase. For the estimations quoted in the main text we have assumed two identical barriers, *i.e.* $\tau_L = \tau_R = \tau$.

Magnetic field effect. Information on the ABSs spin structure can be inferred from their behavior in the presence of a finite magnetic field. This behavior depends strongly on the orientation of the field with respect to the nanowire axis [24]. We consider a magnetic field lying in the xy -plane. The y -component B_y (parallel to the spin states of the transverse subbands without RSO) shifts the energy of the subbands depending on the spin states and modifies the Fermi wave vectors as illustrated in Fig. 6(c). They thus satisfy

$$E_s(k_F) = \frac{\hbar^2 k_F^2}{2m^*} + \frac{E_1^\perp + E_2^\perp}{2} - \sqrt{\left[\frac{E_1^\perp - E_2^\perp}{2} - s \left(\alpha k_F - \frac{g\mu_B}{2} B_y \right) \right]^2} + \eta^2 = \mu. \quad (14)$$

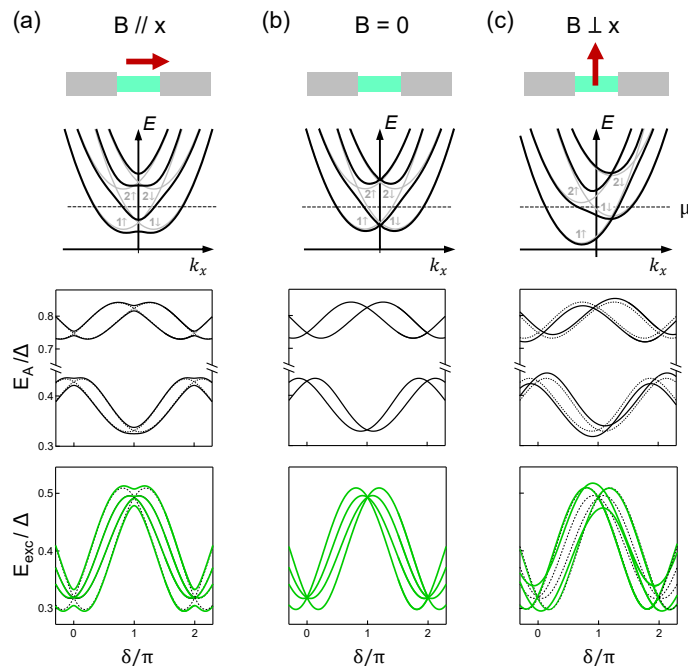


FIG. 6. Effect of an in-plane magnetic field on the band structure (top row), the Andreev levels (middle row) and the excitation spectrum (bottom row). (b) reference graphs at zero field; (a) field applied along the wire axis; (c) field applied perpendicularly to the wire axis.

On the other hand, the x -component B_x mixes opposite-spin states thus opening a gap at the crossings points as illustrated in Fig. 6(a). We include this effect perturbatively[24]. For both, $B//x$ and $B \perp x$ cases, the resulting ABS and the corresponding transition lines are shown in the middle and bottom rows of Fig. 6. In order to fit the data shown in Fig. 4 and Fig. 5, we used $g = 12$, which is within the range of values reported in the literature [39, 40]. Whereas this value gives the best fits of the data at $B \perp x$, better agreement for the data at $B//x$ are obtained with $g = 10$. This could indicate a small anisotropy of the g -factor [40].

Fitting strategy The transcendental equations (Eqs. (1) and (12)) for the single and double barrier models contain dimensionless parameters with which we fit the experimental data:

- $\lambda_1, \lambda_2, \tau$, and x_r for the single barrier model,
- $\lambda_1, \lambda_2, \tau$, and φ_{tot} for the double barrier model.

We then deduce the physical parameters, α, μ (measured from the bottom of the lowest band), L , and U_0 (or $U_{L/R}$) using Eqs. (2), (5) and (11), and assuming that the nanowire diameter is fixed at $W = 140$ nm according to the experimental observation. We further set $m^* = 0.023 m_e$ where m_e is the bare electron mass. For the experimental data in Fig. 4, the single barrier model gives $\lambda_1 = 1.3, \lambda_2 = 2.3, \tau = 0.295$, and $x_r = 0.52$, resulting in the microscopic parameters $\alpha = 53$ meV nm, $\mu = 255 \mu\text{eV}$, $U_0 = 92$ meV nm, $L = 332$ nm. Using the double barrier model, we get $\lambda_1 = 1.1, \lambda_2 = 1.9, \tau = 0.52, \varphi_{\text{tot}} = 0.93 \pmod{2\pi}$, $\alpha = 36$ meV nm, $\mu = 427 \mu\text{eV}$, $U_L = U_R = 130$ meV nm, $L = 314$ nm. Another possibility is to fix the length of the junction L to the length of the uncovered section of the InAs nanowire, 370 nm, which leads to $\alpha = 38$ meV nm and $\mu = 422 \mu\text{eV}$ for the single barrier model ($\alpha = 32$ meV nm and $\mu = 580 \mu\text{eV}$ for the double barrier model). However, in the single barrier model one cannot find values of U_0 leading to the corresponding τ . This is due to the fact that in our simplified model for the scattering matrix, processes involving the higher subbands are neglected, thus limiting its validity to small values of U_0 .

Mod. Phys. **76**, 411 (2004).

- [2] C. W. J. Beenakker and H. van Houten, “Josephson supercurrent through a superconducting quantum point contact shorter than the coherence length”, Phys. Rev. Lett. **66**, 3056 (1991).
- [3] A. Furusaki and M. Tsukada, “Dc Josephson effect

* Corresponding author : hugues.pothier@cea.fr

[1] A. A. Golubov, M. Y. Kupriyanov, and E. Ilichev, “The current-phase relation in Josephson junctions”, Rev.

- and Andreev reflection”, *Solid State Commun.* **78**, 299 (1991).
- [4] P. F. Bagwell, “Suppression of the Josephson current through a narrow, mesoscopic, semiconductor channel by a single impurity”, *Phys. Rev. B* **46**, 12573 (1992).
- [5] J.-D. Pillet, C. H. L. Quay, P. Morfin, C. Bena, A. Levy Yeyati, and P. Joyez, “Revealing the electronic structure of a carbon nanotube carrying a supercurrent”, *Nat. Phys.* **6**, 965 (2010).
- [6] L. Bretheau, Ç. Ö. Girit, H. Pothier, D. Esteve, and C. Urbina, “Exciting Andreev pairs in a superconducting atomic contact”, *Nature* **499**, 312 (2013).
- [7] L. Bretheau, Ç. Ö. Girit, C. Urbina, D. Esteve, and H. Pothier, “Supercurrent spectroscopy of Andreev states”, *Phys. Rev. X* **3**, 041034 (2013).
- [8] C. Janvier, L. Tosi, L. Bretheau, Ç. Ö. Girit, M. Stern, P. Bertet, P. Joyez, D. Vion, D. Esteve, M. F. Goffman, H. Pothier, and C. Urbina, “Coherent manipulation of Andreev states in superconducting atomic contacts”, *Science* **349**, 1199 (2015).
- [9] E. J. H. Lee, X. Jiang, M. Houzet, R. Aguado, C. M. Lieber, and S. De Franceschi, “Spin-resolved Andreev levels and parity crossings in hybrid superconductor-semiconductor nanostructures”, *Nat. Nanotech.* **9**, 79 (2014).
- [10] D. J. van Woerkom, A. Proutski, B. van Heck, Daniël Bouman, J. I. Väyrynen, L. I. Glazman, P. Krogstrup, J. Nygård, L. P. Kouwenhoven, Attila Geresdi, “Microwave spectroscopy of spinful Andreev bound states in ballistic semiconductor Josephson junctions”, *Nature Physics* **13**, 876 (2017).
- [11] M. Hays, G. de Lange, K. Serniak, D. J. van Woerkom, D. Bouman, P. Krogstrup, J. Nygård, A. Geresdi, and M. H. Devoret, “Direct microwave measurement of Andreev-bound-state dynamics in a proximitized semiconducting nanowire”, *Phys. Rev. Lett.* **121**, 047001 (2018).
- [12] S. De Franceschi, L. P. Kouwenhoven, C. Schönberger, and W. Wernsdorfer, “Hybrid superconductor - quantum dot devices”, *Nat. Nanotech.* **5**, 703 (2010).
- [13] Jacob Linder and Jason W. A. Robinson, “Superconducting spintronics”, *Nature Physics* **11**, 307 (2015).
- [14] Elsa Prada, Ramón Aguado, and Pablo San-Jose, “Measuring Majorana nonlocality and spin structure with a quantum dot”, *Phys. Rev. B* **96**, 085418 (2017).
- [15] A. Zazunov, R. Egger, M. Alvarado, and A. Levy Yeyati, “Josephson effect in multiterminal topological junctions”, *Phys. Rev. B* **96**, 024516 (2017).
- [16] M. T. Deng, S. Vaitiekenas, E. Prada, P. San-Jose, J. Nygård, P. Krogstrup, R. Aguado, and C. M. Marcus, “Nonlocality of Majorana modes in hybrid nanowires”, *Phys. Rev. B* **98**, 085125 (2018).
- [17] Sean Hart, Hechen Ren, Michael Kosowsky, Gilad Ben-Shach, Philipp Leubner, Christoph Brüne, Hartmut Buhmann, Laurens W. Molenkamp, Bertrand I. Halperin and Amir Yacoby, “Controlled finite momentum pairing and spatially varying order parameter in proximitized HgTe quantum wells”, *Nat. Phys.* **13**, 87 (2017).
- [18] N. M. Chtchelkatchev and Y. V. Nazarov, “Andreev quantum dots for spin manipulation”, *Phys. Rev. Lett.* **90**, 226806 (2003).
- [19] C. Padurariu and Y. V. Nazarov, “Theoretical proposal for superconducting spin qubits”, *Phys. Rev. B* **81**, 144519 (2010).
- [20] B. Béri, J. H. Bardarson, and C. W. J. Beenakker, “Splitting of Andreev levels in a Josephson junction by spin-orbit coupling”, *Phys. Rev. B* **77**, 045311 (2008).
- [21] Jorge Cayao, Elsa Prada, Pablo San-Jose, and Ramón Aguado, “SNS junctions in nanowires with spin-orbit coupling: Role of confinement and helicity on the sub-gap spectrum”, *Phys. Rev. B* **91**, 024514 (2015).
- [22] B. van Heck, J. I. Väyrynen, and L. I. Glazman, “Zeeman and spin-orbit effects in the Andreev spectra of nanowire junctions”, *Phys. Rev. B* **96**, 075404 (2017).
- [23] C. H. L. Quay, T. L. Hughes, J. A. Sulpizio, L. N. Pfeiffer, K. W. Baldwin, K. W. West, D. Goldhaber-Gordon and R. de Picciotto, “Observation of a one-dimensional spin-orbit gap in a quantum wire”, *Nature Phys.* **6**, 336 (2010).
- [24] Sunghun Park and A. Levy Yeyati, “Andreev spin qubits in multichannel Rashba nanowires”, *Phys. Rev. B* **96**, 125416 (2017).
- [25] M. Governale and U. Zülicke, “Spin accumulation in quantum wires with strong Rashba spin-orbit coupling”, *Phys. Rev. B* **66**, 073311 (2002).
- [26] A. A. Reynoso, G. Usaj, C. A. Balseiro, D. Feinberg, and M. Avignon, “Spin-orbit-induced chirality of Andreev states in Josephson junctions”, *Phys. Rev. B* **86**, 214519 (2012).
- [27] T. Yokoyama, M. Eto, and Y. V. Nazarov, “Anomalous Josephson effect induced by spin-orbit interaction and Zeeman effect in semiconductor nanowires”, *Phys. Rev. B* **89**, 195407 (2014).
- [28] A. Murani, A. Chepelianskii, S. Guéron, and H. Bouchiat, “Andreev spectrum with high spin-orbit interactions: revealing spin splitting and topologically protected crossings”, *Phys. Rev. B* **96**, 165415 (2017).
- [29] M. Zgirski, L. Bretheau, Q. Le Masne, H. Pothier, D. Esteve, and C. Urbina, “Evidence for long-lived quasiparticles trapped in superconducting point contacts”, *Phys. Rev. Lett.* **106**, 257003 (2011).
- [30] Jukka I. Väyrynen, Gianluca Rastelli, Wolfgang Belzig, and Leonid I. Glazman, *Phys. Rev. B* **92**, 134508 (2015).
- [31] P. Krogstrup, N. L. B. Ziino, W. Chang, S. M. Albrecht, M. H. Madsen, E. Johnson, J. Nygård, C. M. Marcus and T. S. Jespersen., “Epitaxy of semiconductor-superconductor nanowires”, *Nat. Mater.* **14**, 400 (2015).
- [32] W. Chang, S. M. Albrecht, T. S. Jespersen, F. Kuemmeth, P. Krogstrup, J. Nygård and C. M. Marcus, “Hard gap in epitaxial semiconductor-superconductor nanowires”, *Nature Nanotechnology* **10**, 232 (2015).
- [33] M. F. Goffman, C. Urbina, H. Pothier, J. Nygård, C. M. Marcus, and P. Krogstrup, “Conduction channels of an InAs-Al nanowire Josephson weak link”, *New J. Phys.* **19**, 092002 (2017).
- [34] C. Fasth, A. Fuhrer, L. Samuelson, Vitaly N. Golovach, and Daniel Loss, “Direct Measurement of the Spin-Orbit Interaction in a Two-Electron InAs Nanowire Quantum Dot”, *Phys. Rev. Lett.* **98**, 266801 (2007).
- [35] Zoltán Scherübl, Gergo Fülöp, Morten H. Madsen, Jesper Nygård, and Szabolcs Csonka, “Electrical tuning of Rashba spin-orbit interaction in multigated InAs nanowires”, *Phys. Rev. B* **94**, 035444 (2016).
- [36] The perfect symmetry of the spectrum when the field is applied parallel to the wire was used to define precisely the field angle, in agreement within a few degrees with a determination from the images of the sample.
- [37] V. E. Degtyarev, S. V. Khazanova and N. V. Demarina,

- “Features of electron gas in InAs nanowires imposed by interplay between nanowire geometry, doping and surface states”, *Scientific Reports* **7**, 3411 (2017).
- [38] M. A. Despósito and A. Levy Yeyati, “Controlled dephasing of Andreev states in superconducting quantum point contacts”, *Phys. Rev. B* **64**, 140511(R) (2001).
- [39] M. T. Björk, A. Fuhrer, A. E. Hansen, M. W. Larsson, L. E. Fröberg, L. Samuelson, “Tunable effective g-factor in InAs nanowire quantum dots”, *Phys. Rev. B* **72**, 201307 (2005).
- [40] S. Vaitiekenas, M.-T. Deng, J. Nygård, P. Krogstrup, and C. M. Marcus, “Effective g Factor of Subgap States in Hybrid Nanowires”, *Phys. Rev. Lett.* **121**, 037703 (2018).
- [41] C.H.L. Quay, M. Weideneder, Y. Chiffaudel, C. Strunk, and M. Aprili, *Nat. Commun.* **6**, 8660 (2015).